Journal of Alloys and Compounds 513 (2012) 566–572

Contents lists available at SciVerse ScienceDirect

Journal of Alloys and Compounds

journal homepage: www.elsevier.com/locate/jallcom

Hydrogen storage and electrochemical characteristics of $Ti_{0.32}Cr_{0.43-x}V_{0.25}Fe_x$ (x = 0–0.08) alloys and its composites with $LmNi_{4.1}Al_{0.25}Mn_{0.3}Co_{0.65}$ alloy

Han-Sol Park, Muralidhar Chourashiya, Dong-Cheol Yang, Choong-Nyeon Park, Chan-Jin Park*

Department of Materials Science and Engineering, Chonnam National University, 77, Yongbong-ro, Buk-gu, Gwangju 500-757, Republic of Korea

ARTICLE INFO

Article history:
Received 15 September 2011
Received in revised form 2 November 2011
Accepted 2 November 2011
Available online 11 November 2011

Keywords:
Ti–Cr–V alloy
Hydrogen storage
Plateau pressure
Fe substitution
Ball-milling
Discharge capacity
Surface catalytic activity

ABSTRACT

This study examined the hydrogen storage and electrochemical characteristics of bcc type $Ti_{0.32}Cr_{0.43-x}V_{0.25}Fe_x$ (x = 0–0.08) alloys and their ball-milled composites with AB_5 type $LmNi_{4.1}Al_{0.25}Mn_{0.3}Co_{0.65}$ alloy. With increasing Fe content in the bcc alloy, the hydrogen storage capacity decreased and the plateau pressure increased due to the decreased lattice volume. In addition, the plateau pressure of the bcc alloys decreased with decrease in its temperature. The discharge capacity of the composite alloys of bcc and AB_5 alloy decreased with increasing Fe content in the bcc alloy at 25 °C, attributed to the increased plateau pressure. On the other hand, at low temperatures, the discharge capacity of the Fe-doped composite alloys was higher than that of the un-doped alloy due to the catalytic effect of Fe. In addition, with increasing discharge rate, the Fe-doped composite alloys with improved surface catalytic activity showed better discharge capacity.

1. Introduction

Commercial Ni-MH secondary batteries employ AB_5 type hydrogen storage alloys as anode materials. However, continuous efforts have been made for new and high-performance anode materials to improve the energy density of Ni-MH secondary batteries [1–13]. In particular, body centered cubic (bcc) structured Ti/V base alloys are potential anode materials for Ni-MH secondary battery owing to their high effective hydrogen storage capacities (>2 wt%) in the desired plateau pressure range (0.01–1 atm) [14–18]. Several previous studies on the absorption and desorption of gas phase hydrogen in the Ti–Cr–V bcc alloys have been reported [15,13,19,20]. In these studies, the Ti–Cr–V bcc alloy exhibited the reversible absorption and desorption of hydrogen near at room temperature. This indicates that the Ti–Cr–V alloy can be successfully employed as a hydrogen storage medium near at room temperature. On the other hand, the alloys remain inactive and show low catalytic activity for the charge-transfer reaction due to the formation of a dense oxide film on Ti or V based alloys in alkaline solutions [18,21]. Accordingly, the discharge capacity of the alloys is much lower than their theoretical discharge capacity in alkaline solutions.

In previous studies, the catalytic activity and discharge capacity of bcc type $Ti_{0.32}Cr_{0.43}V_{0.25}$ alloy were improved either by ball-milling the alloy with the more active AB_5 type $LmNi_{4.1}Al_{0.25}Mn_{0.3}Co_{0.65}$ (Lm: lanthanum-rich mischmetal) alloy [22–25] or by substituting Mn for Cr in the alloy and ball-milling it with an AB_5 type alloy [14]. The more active $LmNi_{4.1}Al_{0.25}Mn_{0.3}Co_{0.65}$ (Lm: lanthanum-rich mischmetal) alloy was embedded in the surface of the $Ti_{0.32}Cr_{0.43}V_{0.25}$ base alloy through the ball-milling thereby forming a path for hydrogen penetration into the bcc alloy. Ball-milling the bcc alloy with a 20 wt% AB_5 alloy for 20 min resulted in a significantly improved discharge capacity of 310 mAh/g. In addition, for further improvement in the catalytic activity of the $Ti_{0.32}Cr_{0.43}V_{0.25}$ alloy, Cr was substituted partially by the more active Mn in the alloy and then ball-milled with the AB_5 alloy. The Mn substituted $Ti_{0.32}Cr_{0.38}Mn_{0.05}V_{0.25}$ alloy after ball-milling with 20 wt% AB_5 exhibited a high discharge capacity of 340 mAh/g. These results encouraged Fe as a new additive for bcc alloys [26–28], which is more cost-effective than Mn while more abundant and active than Cr [20,19].

This study examined the effect of the substitution of Fe for Cr in bcc type $Ti_{0.32}Cr_{0.43-x}V_{0.25}Fe_x$ (x = 0–0.08) alloys and ball-milling the alloys with AB_5 type $LmNi_{4.1}Al_{0.25}Mn_{0.3}Co_{0.65}$ alloy on their hydrogen storage and electrochemical characteristics. Furthermore, the effect of temperature on the electrochemical characteristics of the composites of the bcc and AB_5 alloys were examined.

2. Experimental

Button type ingots of $Ti_{0.32}Cr_{0.43-x}V_{0.25}Fe_x$ (x = 0, 0.03, 0.05 and 0.08) alloys and $LmNi_{4.1}Al_{0.25}Mn_{0.3}Co_{0.65}$ alloy were prepared by an arc-melting method in an argon atmosphere. Each button ingot, weighing approximately 30 g, was re-melted five

* Corresponding author. Tel.: +82 62 530 1704; fax: +82 62 530 1699.
E-mail address: parkcj@chonnam.ac.kr (C.-J. Park).

0925-8388/$ – see front matter © 2011 Elsevier B.V. All rights reserved.
doi:10.1016/j.jallcom.2011.11.010

times to improve the homogeneity of the ingots. The alloys were heated to 1380 °C at a rate of 20 °C/min, held at that temperature for 1 min, and then water quenched immediately. The ingots were crushed mechanically to make alloy powders with a size range of 100–300 μm. The $Ti_{0.32}Cr_{0.43-x}V_{0.25}Fe_x$ (x = 0–0.08) alloy powders were ball-milled with 20 wt% $LmNi_{4.1}Al_{0.25}Mn_{0.3}Co_{0.65}$ alloy powder for 20 min. The detail of ball-milling procedure is reported elsewhere [14]. These mixed alloys are referred as composite alloys, hereinafter.

The crystal structure of the prepared alloys was analyzed by X-ray diffraction (XRD-Panalytical X'pert pro multipurpose X-ray diffractometer with Cu-target). The surface morphology and chemical composition of alloys were observed by field emission scanning electron microscopy (FE-SEM-JSM-7500F) and energy dispersive spectroscopy (EDS-Oxford), respectively. Approximately 1 g of the alloy powder (100–300 μm size) was used to measure the pressure–composition isotherms (PCT) using a Sivert's type apparatus.

Paste type electrodes were fabricated by mixing the composite alloy powder, hydroxyl propyl methyl cellulose (HPMC), 503H binder and carbon black. The resulting slurry was then pasted onto foamed nickel gauze. This nickel foam was then dried and cut into 20 mm × 20 mm sections and used as the working electrode in a cell. The electrochemical cell consisted of a composite alloy as the working electrode, a Pt-wire as the counter electrode and a Hg/HgO as the reference electrode in a 6 M KOH electrolyte. The hydrogen capacity of the bcc Ti-based alloys was approximately 2 wt%, which corresponds to 500 mAh g^{-1} for the electrode. Therefore, the electrodes were charged for 10 h at 50 mA, and were maintained for 5 min under open-circuit conditions after each charging and discharging step. The cut-off voltage for discharge was −650 mV vs. Hg/HgO.

Furthermore, potentiodynamic polarization tests were carried out at a scan rate of 1 mV/s to determine the effect of Fe substitution for Cr on the chemical stability of the alloy.

3. Results and discussion

3.1. Phase analysis of $Ti_{0.32}Cr_{0.43-x}V_{0.25}Fe_x$ (x = 0–0.08) and ball-milled composite alloys

Fig. 1(a) shows the XRD patterns of the $Ti_{0.32}Cr_{0.43-x}V_{0.25}Fe_x$ (x = 0–0.08) alloys, $LmNi_{4.1}Al_{0.25}Mn_{0.3}Co_{0.65}$ alloy and ball-milled composite alloys of $Ti_{0.32}Cr_{0.43-x}V_{0.25}Fe_x$ and $LmNi_{4.1}Al_{0.25}Mn_{0.3}Co_{0.65}$. The as-prepared and composite alloys showed a bcc crystal structure. On the other hand, the peaks in the XRD were observed to shift to the right with increasing Fe content, which is due to a compression in the lattice volume (i.e. decrease in the lattice parameter, as shown in Fig. 1(b)). The linear decrease in the lattice parameter with increasing Fe content was attributed to the comparably smaller atomic radius of Fe than Cr. For simplicity, the $Ti_{0.32}Cr_{0.43-x}V_{0.25}Fe_x$ (x = 0–0.08) alloy will be referred hereinafter as a "bcc" alloy.

An analysis of the XRD pattern of the $LmNi_{4.1}Al_{0.25}Mn_{0.3}Co_{0.65}$ alloy powder confirmed its $CaCu_5$ (AB_5) type crystal structure. The XRD pattern of the composite alloys did not reveal any indication of AB_5 alloys, which can be attributed to the formation of an amorphous/nano-sized AB_5 alloy during the ball milling. Moreover, the bcc alloys preserved its crystalline nature, even after ball-milling, which can be attributed to the comparably less brittle nature of the bcc alloy than that of the AB_5 alloy. On the other hand, a comparison of the XRD peak broadness of the as-prepared alloys and that of the composite alloy revealed grain-size refinement in the ball-milled composite alloys.

Fig. 2 shows the typical back-scattered electron (BSE) image of a ball-milled composite alloy with spot-EDS analysis. The BSE image of ball-milled composite alloy clearly indicated the presence of two phases, one phase forming the bulk and the other partially covering the bulk-phase. The point EDS at the regions with different contrast (marked as 'a' (darker) and 'b' (brighter)) clarified the phase-composition. The estimated composition percentage for bcc and AB_5 for the respective regions are mentioned in the inset table of the respective spot-EDS, which confirms that the brighter region consists of AB_5 phase while the dark region corresponds to the bcc alloy. The AB_5 phase on the surface of the bcc alloy can act as a path for the diffusion of hydrogen.

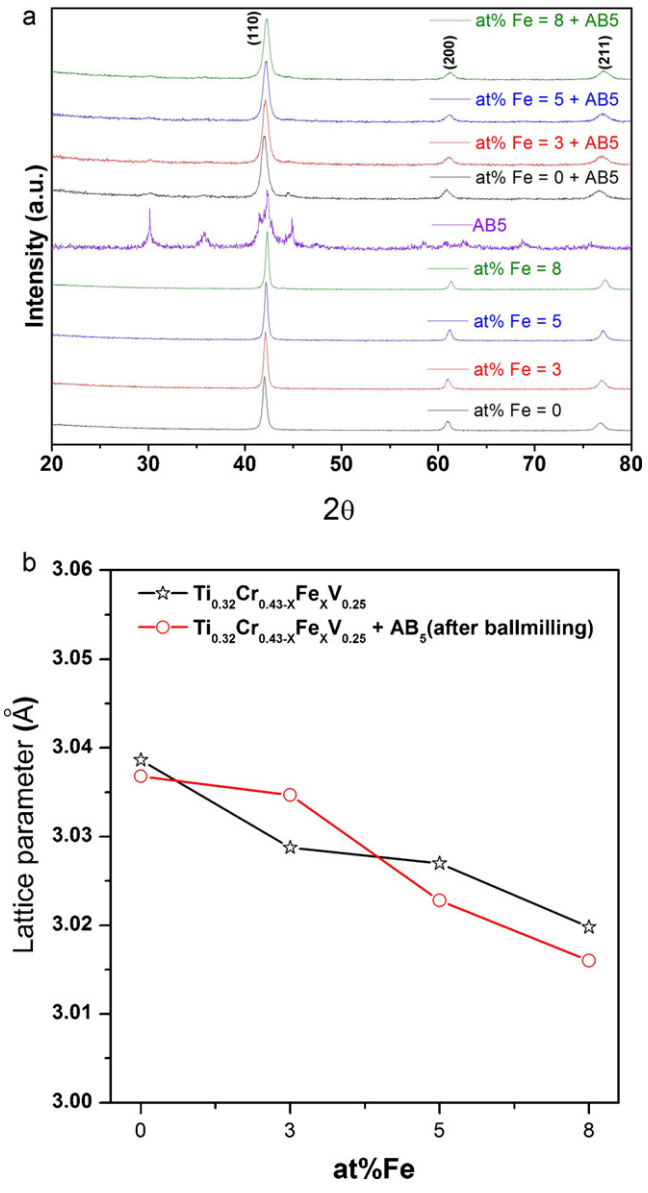

Fig. 1. (a) XRD patterns of $Ti_{0.32}Cr_{0.43-x}V_{0.25}Fe_x$ (x = 0–0.08), $LmNi_{4.1}Al_{0.25}Mn_{0.3}Co_{0.65}$, ball-milled composite alloys and (b) variation of the lattice parameter.

3.2. Effect of the Fe content and temperature on the hydrogen storage characteristics of $Ti_{0.32}Cr_{0.43-x}V_{0.25}Fe_x$ (x = 0–0.08) alloys

The pressure–composition-isotherms (PCT) of the alloys were obtained to examine the effects of the Fe content and temperature on the hydrogen absorption–desorption characteristics of intrinsic $Ti_{0.32}Cr_{0.43-x}V_{0.25}Fe_x$ (x = 0–0.08) alloys, as shown in Fig. 3. From the PCT curves, the maximum hydrogen capacities are defined as the amount of hydrogen absorbed at a hydrogen pressure of 5 MPa and the effective hydrogen capacities as the amount of hydrogen desorbed from 5 MPa to 20 kPa. With increasing Fe content in the bcc alloys, the maximum and effective hydrogen capacities decreased at 25 °C, which was attributed to the decrease in the lattice-parameter/lattice-volume of the bcc alloys with the Fe content, as shown in Fig. 1(b).

Furthermore, Fig. 4 shows the change in the plateau pressure (P_{eq}) obtained from the PCT curves of the bcc alloys measured at different temperatures (T) and the corresponding log P_{eq} vs. $1/T$ plots. The plateau pressure of each alloy decreased with decreasing

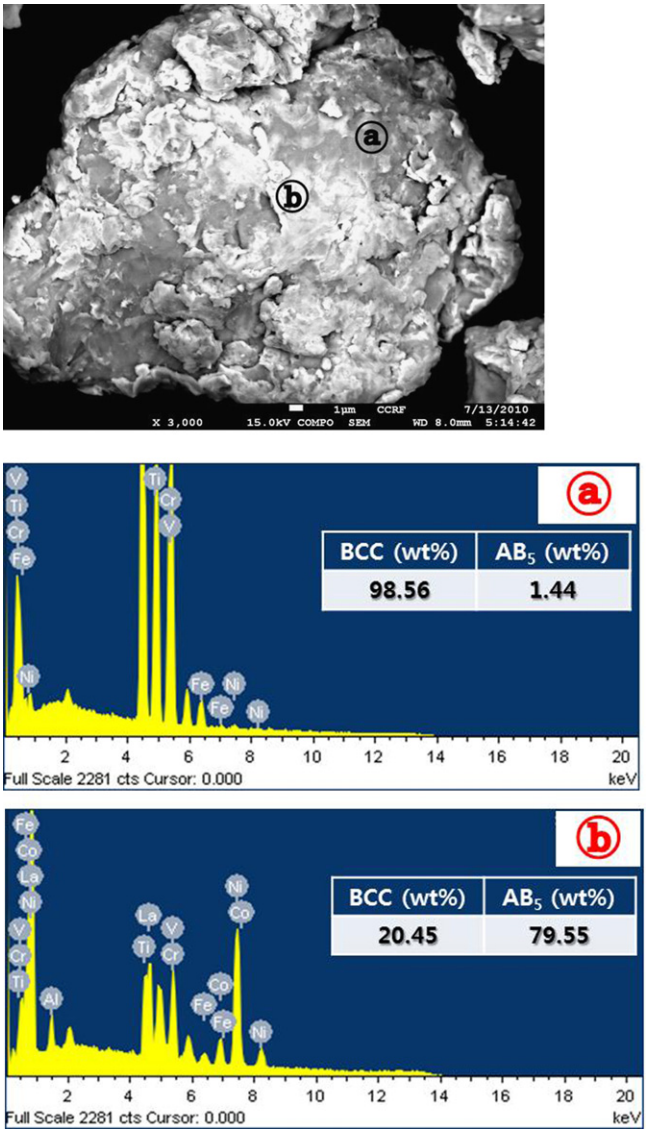

Fig. 2. Typical back scattered electron (BSE) image of the ball-milled composite alloy ($Ti_{0.32}Cr_{0.38}V_{0.25}Fe_{0.05} + AB_5$) and point EDS spectrums at marked positions.

temperature, whereas the maximum hydrogen capacity increased, as shown in Fig. 3. This is in accordance with the van't Hoff equation, which states that $\ln P_{eq}$ is inversely proportional to temperature.

3.3. *Effect of temperature on discharge capacities of ball-milled composite alloy electrodes*

The electrodes were prepared using the alloys and tested in a 6 M KOH solution to examine the adoptability of the alloys as an anode material for Ni-MH batteries. Before all measurements of the discharge capacity for the electrodes under different test conditions, the electrodes were activated for seven cycles at 25 °C by repeatedly charging and discharging at a 0.1 C-rate. Fig. 5 shows the discharge capacities of the $Ti_{0.32}Cr_{0.43-x}V_{0.25}Fe_x$ ($x = 0$–0.08) alloy electrodes without AB_5 additives. Un-doped and Fe doped bcc alloys exhibited much lower discharge capacity than their theoretical values, which can be attributed to the formation of Ti- or V-rich oxide layers on the surface of the as-prepared alloys in a KOH solution, inhibiting the absorption of hydrogen during charging [21,22].

To enhance the surface activation of the bcc alloys, the alloys were ball-milled with AB_5 type $LMNi_{4.1}Al_{0.25}Mn_{0.3}Co_{0.65}$ alloy.

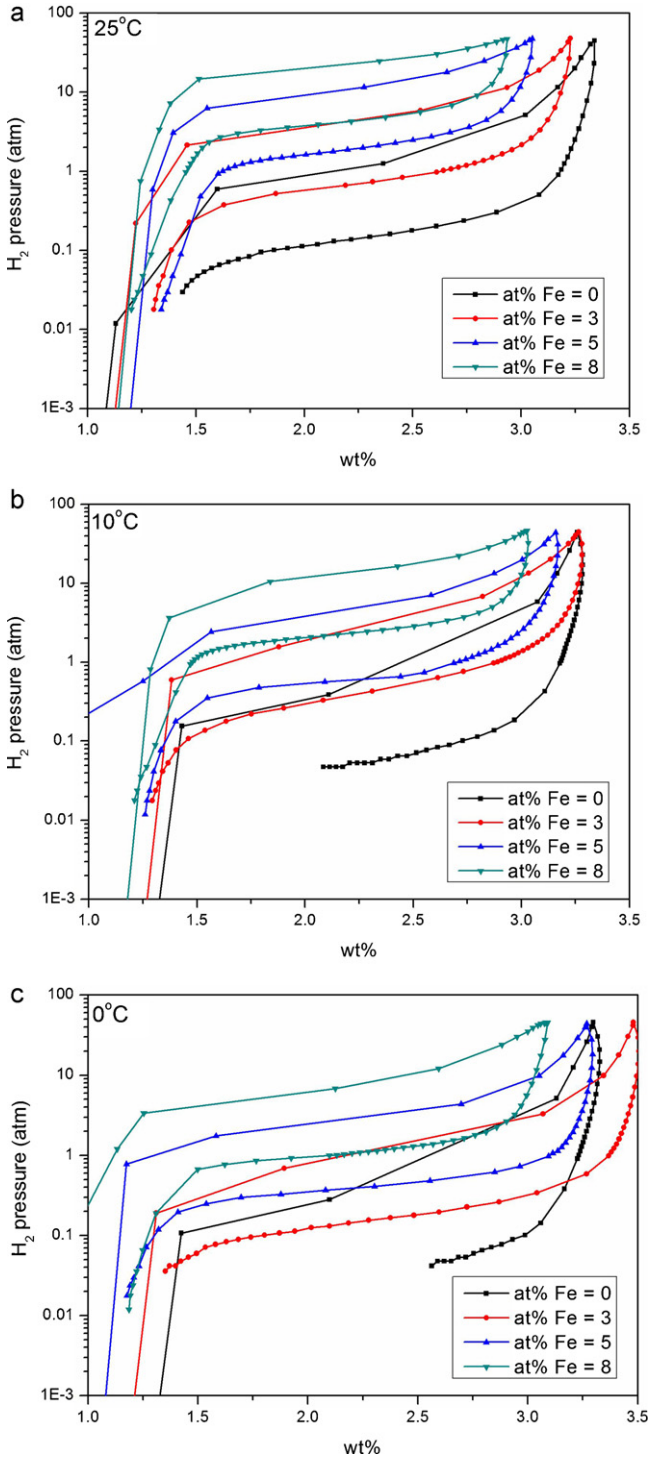

Fig. 3. Pressure–composition isotherms of $Ti_{0.32}Cr_{0.43-x}V_{0.25}Fe_x$ ($x = 0$–0.08) alloys measured at (a) 25 °C, (b) 10 °C and (c) 0 °C.

Fig. 6 shows the discharge capacity of the composite alloys at room and low temperatures. The bcc alloys when ball-milled with AB_5 alloys exhibited a substantial improvement in their discharge capacities, even though their discharge capacities were still lower than their theoretical ones. These results suggest that the surfaces of the bcc alloys were activated by ball-milling with the AB_5 alloy, where surface-attached AB_5 alloy particles, as shown in Fig. 2, act as a path for hydrogen penetration.

Apart from this improvement, the doped composite alloy ($x = 0.03$–0.08) showed lower discharge capacity (<250 mAh/g)

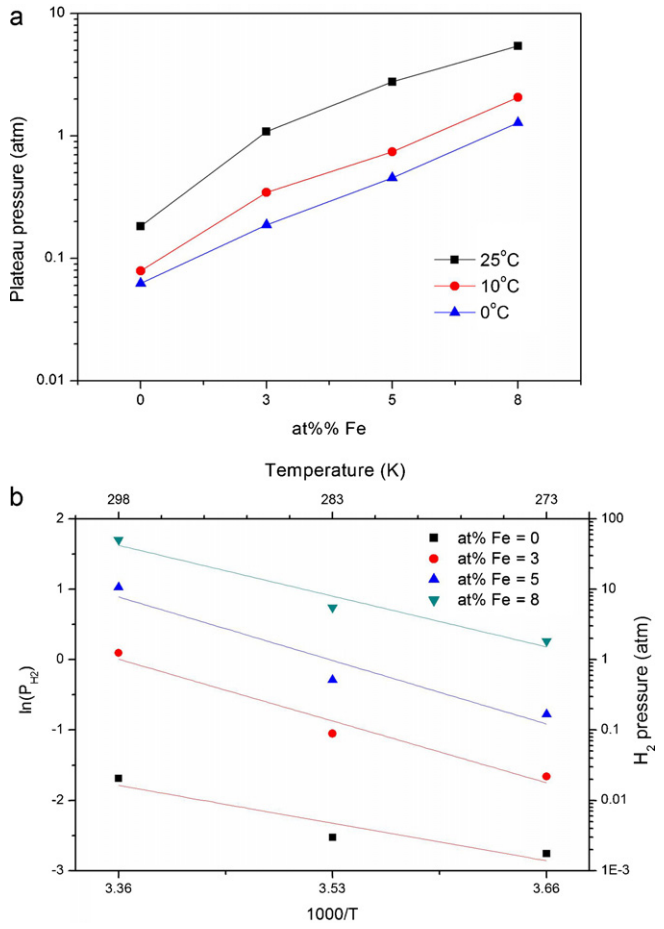

Fig. 4. (a) Variation in the plateau pressure obtained from PCT curves of $Ti_{0.32}Cr_{0.43-x}V_{0.25}Fe_x$ (x = 0–0.08) alloys measured at different temperatures and (b) the corresponding van't Hoff plot.

compared to the un-doped (x = 0) composite alloys (~300 mAh/g) at 25 °C. In particular, the discharge capacity of the Fe doped composite alloy decreased with increasing Fe content. According to Figs. 3 and 4, the plateau pressure of the bcc alloy increased with increasing Fe content. This suggests that for the composite alloys with a high Fe content, the hydrogen-ions from the electrolyte may evolve as hydrogen gas instead of diffusing into the bcc alloy during charging and eventually result in a lower discharge capacity. The measured discharge capacity of the bcc alloy is closely associated with its plateau pressure shown in Fig. 4. Too low plateau pressure of the alloy indicates that the hydrogen absorbed in the alloy is hardly desorbed due to the high lattice binding energy. Thus, the alloy cannot exhibit the good discharge

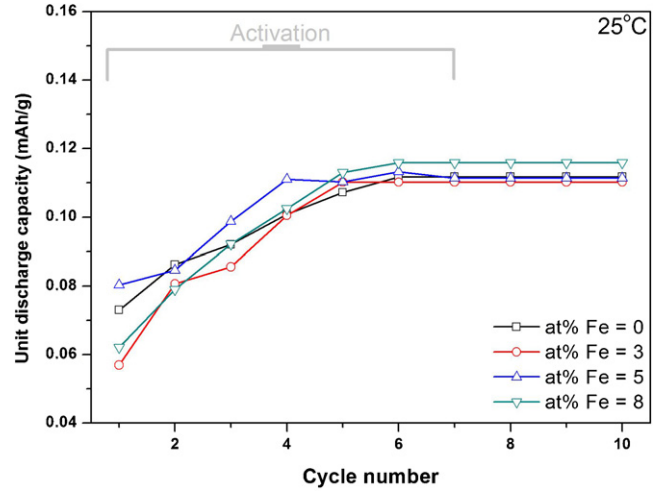

Fig. 5. Discharge capacity of the $Ti_{0.32}Cr_{0.43-x}V_{0.25}Fe_x$ (x = 0–0.08) alloy electrodes measured at 25 °C.

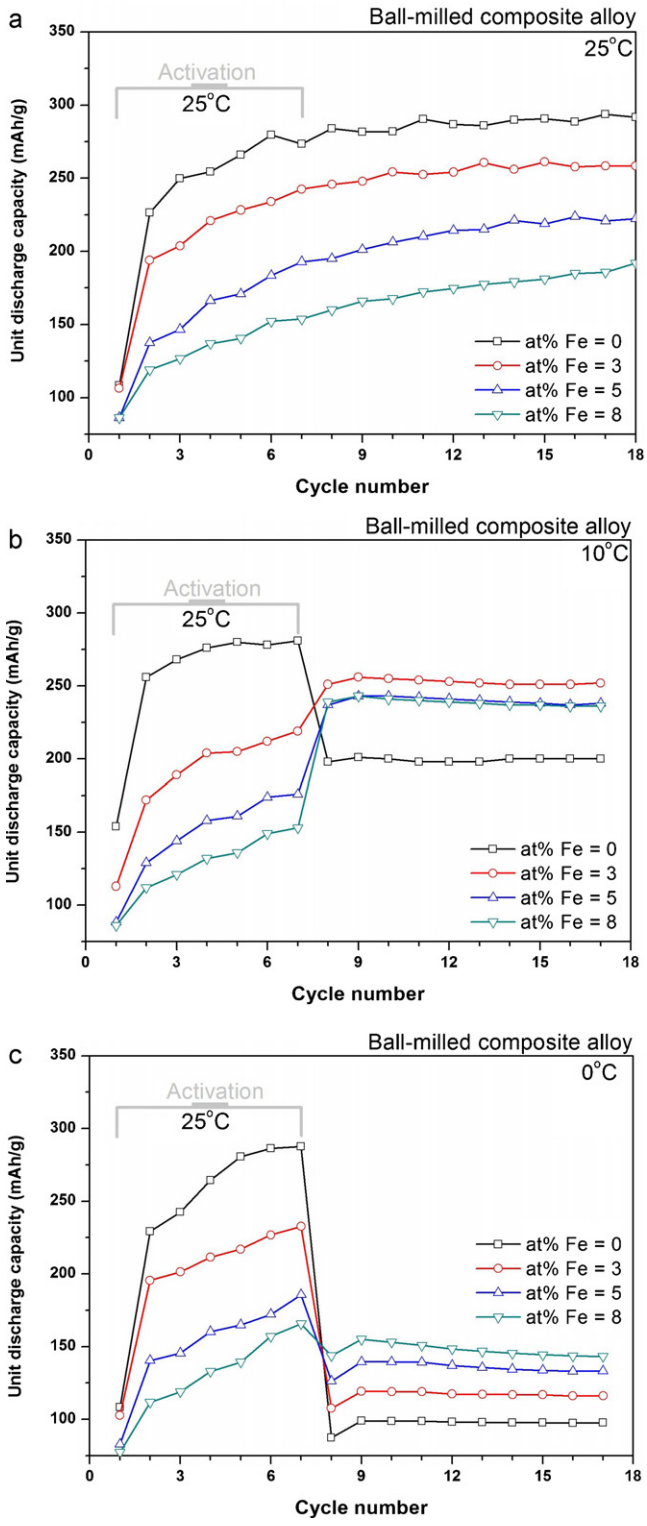

Fig. 6. Discharge capacity of the composite alloy electrodes at (a) 25 °C, (b) 10 °C and (c) 0 °C.

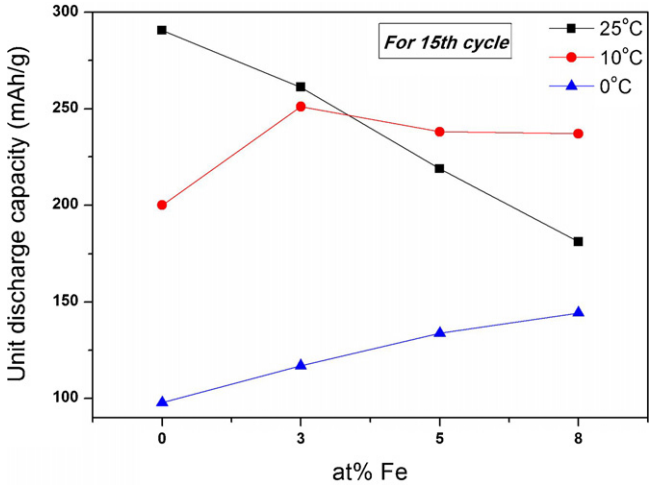

Fig. 7. Variation in the discharge capacities of the composite alloys (15th cycle) as a function of the Fe content.

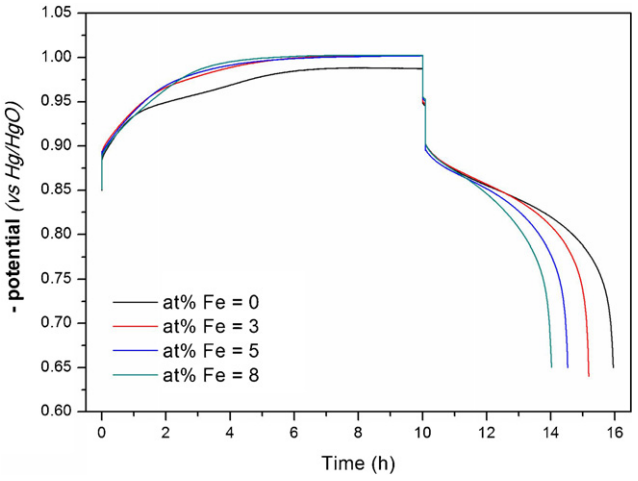

Fig. 8. Potential variation of the composite alloy electrodes during charging and discharging.

capacity. In contrast, too high plateau pressure of the alloy indicates that the hydrogen is hardly absorbed into the alloy and the hydrogen can also be easily released as a hydrogen gas. This also induces the poor charging efficiency and accordingly the low discharge capacity. The plateau pressure range suitable for an anode in Ni-MH battery is 0.01–1 atm.

Fig. 6(a)–(c) also shows the effect of the electrolyte/operating temperature on the discharge capacities of the ball-milled composite alloys. In contrast to the data obtained at room temperature (25 °C), the discharge capacity of the un-doped composite alloy measured at 10 °C and 0 °C was lower than that of the Fe-doped ones. In addition, the discharge capacity of the alloys containing 5 and 8 at% Fe measured at 10 °C was higher than that measured at 25 °C. Interestingly, in the electrolyte at 0 °C, the discharge capacity of the composite alloy electrode increased with increasing Fe content. These variations of discharge capacity can be understood clearly from Fig. 7, where the variation in discharge capacities for the 15th cycle is presented as a function of the Fe content at different temperatures. On the other hand, it should be noted that although the trend is reversed at the lower electrolyte temperature (0 °C), the unit discharge capacities are lower than that of the respective composite alloys with the electrolyte at 25 °C.

The lower discharge capacity of the Fe-doped composite alloy electrodes at 25 °C was attributed to the higher plateau pressure of the alloys (Fig. 3). For the alloy with a high plateau pressure, hydrogen can diffuse out from the alloy and be released as a hydrogen gas during charging. This also degrades the charging efficiency and accordingly the discharge capacity of the electrode. Fig. 8 shows the potential variation of the alloy electrodes during charging and discharging. Although the un-doped electrode exhibited a clear potential drop to the hydrogen evolution potential after finishing the charging process, the Fe-doped electrodes showed no clear potential drop during charging indicating the continuous hydrogen evolution and poor charging efficiency. The poorer

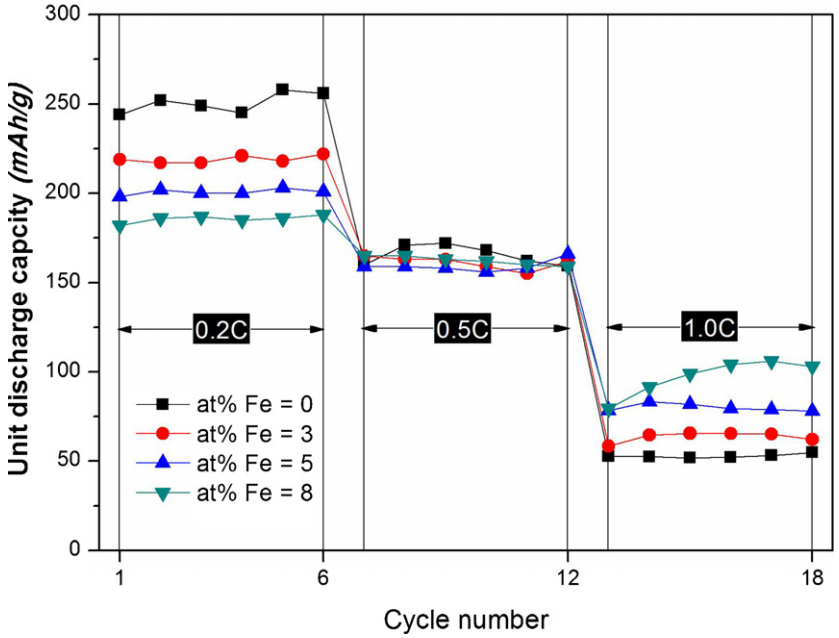

Fig. 9. Effect of the C-rate on the discharge capacity of the composite alloys at 25 °C.

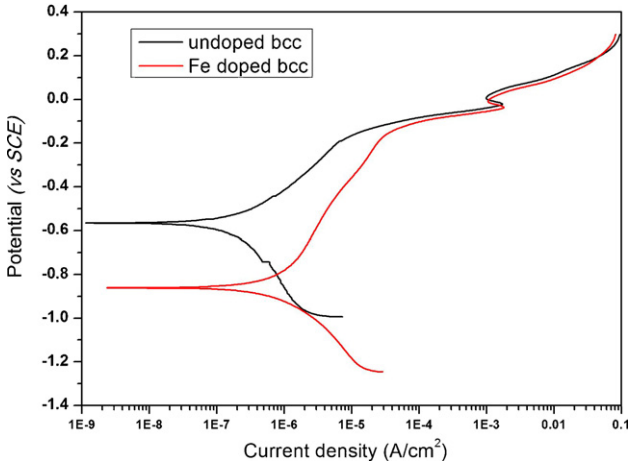

Fig. 10. Potentiodynamic polarization curves of the un-doped and 5 at% Fe-doped alloys.

charging efficiency results in lower discharge capacity. On the other hand, with decreasing temperature, the contribution of the plateau pressure became less important. In particular, at 0 °C, the Fe-doped electrodes might exhibit better catalytic activity for the charge transfer reaction than the un-doped electrode and higher discharge capacity.

3.4. Effect of discharge rate on discharge capacities of ball-milled composite alloys

Fig. 9 shows the effect of the discharge rate on the discharge capacity of the alloy electrodes. During charging, the same charge rate of 0.1 C was applied to all electrodes. The discharge capacity of all electrodes decreased sharply with increasing discharge rate. The degree of polarization increased with increasing discharge current, and the discharge capacity of the electrode decreased. At a 0.2 C-rate, the discharge capacity of the composite alloy decreased with increasing Fe content. As mentioned previously, this phenomenon is closely associated with the increased plateau pressure in the PCT curves with increasing Fe content. The high plateau pressure of the bcc alloy induces poor charging efficiency. On the other hand, at a high C-rate, the discharge capacity was observed to increase with increasing Fe content. This increase in discharge capacity might be due to the increased surface catalytic activity of the electrode by the addition of Fe. With increasing C-rate, the contribution of the activation polarization on the electrode becomes more important. Therefore, the Fe-doped electrodes with the improved surface catalytic activity show better discharge capacity. This trend is similar to that of lower temperature measurements.

3.5. Potentiodynamic polarization behavior of the bcc alloys

Fig. 10 shows a comparison of potentiodynamic curves of the $Ti_{0.32}Cr_{0.43}V_{0.25}$ and $Ti_{0.32}Cr_{0.38}V_{0.25}Fe_{0.05}$ alloys. For the Fe-doped bcc alloy, the corrosion potential was lower and the passive current density was higher than those of the un-doped alloy. This suggests that the Fe-doped alloy is more active and less protective than the un-doped alloy. In particular, considering the fact that the bcc type Ti–Cr–V alloy is barely activated due to the presence of a dense and protective passive film formed spontaneously on the surface of the alloy in an alkaline solution, the higher passive current density of the Fe-doped alloy suggests that that the passive film on a Fe-doped alloy is less stable than that of the un-doped alloy. Therefore, the Fe-doped alloys can be activated easily. This also induces more rapid charge transfer kinetics during the anodic discharge reactions.

4. Conclusions

$Ti_{0.32}Cr_{0.43-x}V_{0.25}Fe_x$ (x = 0–0.08) alloys and their composite (with 20 wt% $LmNi_{4.1}Al_{0.25}Mn_{0.3}Co_{0.65}$ alloy) both exhibited a bcc crystal structure and showed a decrease in its lattice parameter with increasing Fe content. The plateau pressure in PCT curves increased with increase in Fe content in bcc alloys, which is attributed to decrease in lattice parameter, as decreased lattice volume obstructs the diffusion of hydrogen into the lattice. In addition, the plateau pressure of the bcc alloys decreased with decrease in its temperature. The discharge capacity of the composite alloys of bcc and AB_5 alloy decreased with increasing Fe content in the bcc alloy at 25 °C, attributed to the increased plateau pressure. On the other hand, at low temperatures, the discharge capacity of the Fe-doped composite alloys was higher than that of the un-doped alloy due to the catalytic effect of Fe. In addition, with increasing discharge rate, the Fe-doped composite alloys with improved surface catalytic activity showed better discharge capacity.

Acknowledgements

This study was financially supported by the Ministry of Education, Science Technology (MEST) and National Research Foundation of Korea (NRF) through the Basic Research Laboratories (BRL) Program (2011-0001567) and the Human Resource Training Project for Regional Innovation.

References

[1] M.V. Ananth, M. Raju, K. Manimaran, G. Balachandran, L.M. Nair, Journal of Power Sources 167 (2007) 228–233.
[2] S. Shi, C. Ouyang, M. Lei, Journal of Power Sources 164 (2007) 911–915.
[3] J. Shi, F. Wu, D. Hu, S. Chen, L. Mao, G. Wang, Journal of Power Sources 161 (2006) 692–701.
[4] D. Lu, W. Li, S. Hu, F. Xiao, R. Tang, International Journal of Hydrogen Energy 31 (2006) 678–682.
[5] C. Wang, M. Marrero-Rivera, D.A. Serafini, J.H. Baricuatro, M.P. Soriaga, S. Srinivasan, International Journal of Hydrogen Energy 31 (2006) 603–611.
[6] C. Rongeat, M.H. Grosjean, S. Ruggeri, M. Dehmas, S. Bourlot, S. Marcotte, L. Roué, Journal of Power Sources 158 (2006) 747–753.
[7] R. Tang, X. Wei, Y. Liu, C. Zhu, J. Zhu, G. Yu, Journal of Power Sources 155 (2006) 456–460.
[8] E. Jankowska, M. Makowiecka, M. Jurczyk, Journal of Alloys and Compounds 404–406 (2005) 691–693.
[9] F. Feng, D.O. Northwood, International Journal of Hydrogen Energy 30 (2005) 1367–1370.
[10] B. Huang, P. Shi, Z. Liang, M. Chen, Y. Guan, Journal of Alloys and Compounds 394 (2005) 303–307.
[11] Y. Chai, M. Zhao, International Journal of Hydrogen Energy 30 (2005) 279–283.
[12] H. Pan, X. Wu, M. Gao, N. Chen, Y. Yue, Y. Lei, International Journal of Hydrogen Energy 31 (2006) 517–523.
[13] S.-W. Cho, G. Shim, G.-S. Choi, C.-N. Park, J.-H. Yoo, J. Choi, Journal of Alloys and Compounds 430 (2007) 136–141.
[14] J.-Y. Kim, C.-N. Park, J.-S. Shim, C.-J. Park, J. Choi, H. Noh, Journal of Power Sources 180 (2008) 648–652.
[15] S.-W. Cho, C.-N. Park, J.-H. Yoo, J. Choi, J.-S. Park, C.-Y. Suh, G. Shim, Journal of Alloys and Compounds 403 (2005) 262–266.
[16] S.-W. Cho, C.-S. Han, C.-N. Park, E. Akiba, Journal of Alloys and Compounds 289 (1999) 244–250.
[17] E. Akiba, H. Iba, Intermetallics 6 (1998) 461–470.
[18] X.B. Yu, Z. Wu, B.J. Xia, N.X. Xu, Journal of Alloys and Compounds 386 (2005) 258–260.
[19] J.-H. Yoo, G. Shim, S.-W. Cho, C.-N. Park, International Journal of Hydrogen Energy 32 (2007) 2977–2981.
[20] J.-H. Yoo, G. Shim, C.-N. Park, W.-B. Kim, S.-W. Cho, International Journal of Hydrogen Energy 34 (2009) 9116–9121.
[21] X.B. Yu, Z. Wu, B.J. Xia, N.X. Xu, Journal of Alloys and Compounds 375 (2004) 221–223.
[22] J.-Y. Park, C.-N. Park, C.-J. Park, J. Choi, International Journal of Hydrogen Energy 32 (2007) 4215–4219.

[23] X.B. Yu, Applied Physics Letters 87 (2005) 133121.
[24] X.B. Yu, Z. Wu, T.S. Huang, Journal of Alloys and Compounds 476 (2009) 787–790.
[25] X.B. Yu, Z. Wu, B.J. Xia, N.X. Xu, Journal of The Electrochemical Society 151 (2004) A1468–A1472.
[26] X. Yu, Applied Physics Letters 84 (2004) 3199.
[27] X.B. Yu, S.L. Feng, Z. Wu, B.J. Xia, N.X. Xu, Journal of Alloys and Compounds 393 (2005) 128–134.
[28] X.B. Yu, Z.X. Yang, S.L. Feng, Z. Wu, N.X. Xu, International Journal of Hydrogen Energy 31 (2006) 1176–1181.